

Elliptical Polarization of Fe^{57} Gamma Rays*

H. FRAUENFELDER,† D. E. NAGLE, R. D. TAYLOR, D. R. F. COCHRAN, AND W. M. VISSCHER
Los Alamos Scientific Laboratory, University of California, Los Alamos, New Mexico

(Received November 20, 1961)

The Mössbauer effect provides a tool to investigate the angular dependence and the polarization of individual components emitted in the nuclear Zeeman effect. A discussion of the physical picture of the photon polarization in Fe^{57} is followed by the general theory of elliptical polarization in the Mössbauer effect. The experimental arrangement to measure this polarization is described and some relevant results are given.

1. INTRODUCTION

THE observation of splitting and polarization of light emitted in the Zeeman effect has been extremely important in the development of the understanding of atomic structure. In nuclear physics, prior to the discovery of the Mössbauer effect, similar experiments were impossible. It is true that many polarization experiments have been performed with nuclear gamma rays, but these experiments have been difficult and cumbersome. Moreover, they always had to be performed on components unresolved in energy, and the information gathered about the polarization of individual components was rather indirect.

The Mössbauer effect has changed this situation. Particularly with the 14.4-keV gamma ray emitted by Fe^{57} , the nuclear Zeeman effect can be observed easily and in detail.¹⁻³ The individual components of the emitted gamma-ray lines are widely separated and show the natural linewidth. The 93-keV gamma ray in Zn^{67} displays a Zeeman splitting of many linewidths in fields as small as 100 gauss.⁴

Once the Zeeman components are separated clearly, the determination of their state of polarization becomes the next step. Experiments with the plane polarization of the Fe^{57} gamma rays were first performed by the Argonne group in order to completely understand the Mössbauer spectrum of Fe^{57} imbedded in iron.³ The gamma-ray polarization has also been taken into account by Wegener and Obenshain in order to explain the shape of the lines observed in Ni^{61} .⁵ The elliptical polarization was first used to simplify the investigation of the complicated spectra which appear when Fe^{57} is imbedded in CoPd .⁶

These latter experiments led to the present investigation of the production and the measurement of ellipti-

cally polarized gamma rays. Only after the relevant experimental problems are well understood and after the theory has been worked out can the determination of the polarization of gamma rays emitted and absorbed in the Mössbauer effect be used as an effective tool.

Some applications of this tool are obvious. Complex spectra may be unraveled. The number of lines observed in complicated spectra can be reduced and the remaining lines will be more intense. Information about the net direction of magnetization inside magnetic domains in ferromagnets, antiferromagnets, and possibly superconducting ferromagnets can be obtained.

The present paper contains in Sec. 2 a simple description of the polarization effects to be expected in Fe^{57} . In Sec. 3, the general theory is developed. The experimental arrangements and results used to verify the predictions of the theory are treated in Sec. 4. The results are discussed in Sec. 5.

2. THE PHYSICAL PICTURE

Before treating the general theory of the polarization of gamma rays in the Mössbauer effect, a few simple remarks about the case of Fe^{57} will make the physical ideas clearer. Figure 1(a) shows the relevant levels of Fe^{57} imbedded in ferromagnetic iron metal and placed in an external magnetic field. The labeling of the magnetic sublevels corresponds to the convention that the external field is directed along the $+z$ axis and the experimental findings that the field at the Fe^{57} nuclei is opposite to the external field, and that the moment of the 14-keV level is negative⁷ [Fig. 1(b)]. The 14.4-keV gamma ray, emitted to the transition from the first-excited to the ground state, is a magnetic dipole

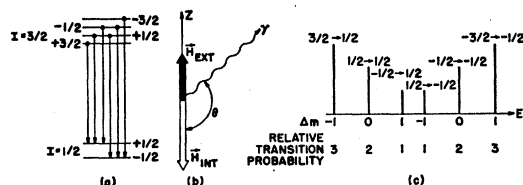


FIG. 1. (a) Zeeman levels of the ground state and the first-excited state of Fe^{57} . (b) Orientation of quantization axis, external and internal magnetic field, and emitted gamma ray in ferromagnetic iron. (c) Zeeman components of Fe^{57} gamma ray.

* Work done under the auspices of the U. S. Atomic Energy Commission.

† Permanent address: Department of Physics, University of Illinois, Urbana, Illinois.

¹ R. V. Pound and G. A. Rebka, *Phys. Rev. Letters* **3**, 554 (1959).

² G. DePasquali, H. Frauenfelder, S. Margulies, and R. N. Peacock, *Phys. Rev. Letters* **4**, 71 (1960).

³ S. S. Hanna, J. Heberle, C. Littlejohn, G. J. Perlow, R. S. Preston, and D. H. Vincent, *Phys. Rev. Letters* **4**, 177 (1960).

⁴ P. P. Craig, D. E. Nagle, and D. R. F. Cochran, *Phys. Rev. Letters* **4**, 561 (1960).

⁵ H. F. Wegener and F. E. Obenshain, *Z. Physik* **163**, 17 (1961).

⁶ D. E. Nagle, H. Frauenfelder, R. D. Taylor, D. R. F. Cochran, and B. T. Matthias, *Phys. Rev. Letters* **5**, 364 (1960).

⁷ S. S. Hanna, J. Heberle, G. J. Perlow, R. S. Preston, and D. H. Vincent, *Phys. Rev. Letters* **4**, 513 (1960).

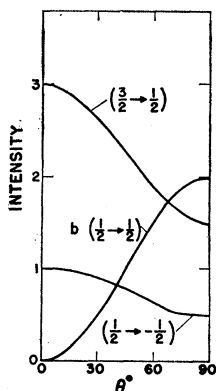


FIG. 2. Relative intensities of the components of the emission or absorption lines of Fe^{57} in a magnetic field as a function of the angle θ between field and direction of propagation. Only three components are shown.

radiation with less than 10^{-4} intensity admixture of electric quadrupole radiation.⁸

The radiation pattern emitted by an unmagnetized Fe^{57} source below its Curie temperature consists of six lines as shown in Fig. 1(c). The intensity of each component is a function of the angle θ between the direction of emission and the direction of the field H_{int} at the nucleus, and it is given by the product of a transition probability and an angular factor.⁹ The transition probabilities are proportional to squares of Clebsch-Gordan coefficients; relative values are given in Fig. 1(c). The angular factors for dipole radiation are treated in texts on electrodynamics; they are

$$F^0(\theta) = 2 \sin^2\theta \quad \text{for } \Delta m = 0,$$

$$F^{\pm 1}(\theta) = 1 + \cos^2\theta \quad \text{for } \Delta m = \pm 1.$$

The relative intensities of the six components of Fig. 1,

$$W\left(\frac{3}{2} \rightarrow \frac{1}{2}\right) = W\left(-\frac{3}{2} \rightarrow -\frac{1}{2}\right) = 3(1 + \cos^2\theta)/2,$$

$$W\left(\frac{1}{2} \rightarrow -\frac{1}{2}\right) = W\left(-\frac{1}{2} \rightarrow \frac{1}{2}\right) = (1 + \cos^2\theta)/2,$$

$$W\left(\frac{1}{2} \rightarrow \frac{1}{2}\right) = W\left(-\frac{1}{2} \rightarrow -\frac{1}{2}\right) = 2 \sin^2\theta,$$

are shown in Fig. 2 as a function of the angle θ .

Before the discovery of recoilless gamma-ray processes, the various components could only be distinguished by their angular distribution and by their polarization, properties which were extensively investigated in angular correlation and nuclear alignment studies. The Mössbauer effect, however, makes it possible to study each component separately and to investigate its directional distribution $F(\theta)$ and its polarization.

The simplest pattern occurs when one is observing along the axis of the external magnetic field. Figures 1 and 2 then show that the emission or absorption pattern

⁸ G. T. Ewan, R. L. Graham, and J. S. Geiger, *Nuclear Phys.* **19**, 221 (1960).

⁹ Obviously, one must know the relative directions of internal and external magnetic field in order to apply the formulas derived in Sec. 3. In ferromagnets, the internal field is opposite to the external one in most cases investigated so far. In thin films, however, the field relations can be more complicated and the polarization measurements can serve as a tool to find the direction of the field at the nucleus.

each consists of only four, instead of six lines. The transition $\Delta m = 0$ is completely extinguished. To discuss the polarization of these four components, we note that a gamma ray is called right-circularly polarized if its spin lies in the direction of motion. (This convention is opposite to the one used in optical spectroscopy.) We consider first the highest energy component in Fig. 1, namely the transition $-\frac{3}{2}$ to $-\frac{1}{2}$. The z component of angular momentum must be conserved, and any gamma ray corresponding to this component hence must have a z component of angular momentum -1 . If this gamma ray is emitted along the $+z$ direction, its spin is antiparallel to its momentum and it is left circularly polarized. If it is emitted in the $-z$ direction, spin and momentum are parallel and the photon is right-circularly polarized. Similarly, one can see that the other components are also circularly polarized.

For directions of emission other than along the magnetic-field axis, the picture is no longer so simple, but the intensities and polarizations of the components can be calculated from the equations of the next section. In particular, at right angles to the field direction, all six components appear, with intensities 3:4:1:1:4:3, and they are linearly polarized (transverse Zeeman effect). At intermediate angles, the components are elliptically polarized.

3. THEORY

3.1. Multipole Expansion of Emission Matrix Element

Although some of the expressions we shall derive in this section may be found in other places,^{5,10} for the sake of completeness, we will start from the assumption that the interaction H of the nucleus with the external electromagnetic field is linear in the vector potential \mathbf{A} ;

$$H = \sum_{\text{nucleons}} \mathbf{A} \cdot \mathbf{j} + \text{Hermitian conjugate}, \quad (1)$$

where \mathbf{j} is defined by Eq. (1) and depends only on the nucleon variables. For our purposes, its form is irrelevant; only the fact that it is a vector will be needed.

The matrix element of H for the emission of a plane wave in the direction \mathbf{k} with polarization \hat{n} (where $\hat{n} \cdot \mathbf{k} = 0$ and a caret denotes a unit vector) may be written (suppressing the sum over nucleons)

$$H_{fi} = (j_f m_f | e^{i\mathbf{k} \cdot \mathbf{r}} \hat{n} \cdot \mathbf{j} | j_i m_i) = \hat{n} \cdot \mathbf{J}_{fi},$$

or

$$\mathbf{J}_{fi} = \sum_{\mu=-1}^1 \hat{h}_{\mu} (j_f m_f | e^{i\mathbf{k} \cdot \mathbf{r}} j^{\mu} | j_i m_i), \quad (2)$$

where we have introduced spherical unit basis vectors \hat{h}_{μ} with \hat{h}_0 in the direction of the axis of quantization. Next, using the Legendre expansion for the exponential,

¹⁰ M. E. Rose, *Multipole Fields* (John Wiley & Sons, Inc., New York, 1955).

TABLE I. Nomenclature for multipole radiation. *E*, *M*, *D*, and *Q* stand for electric, magnetic, dipole, and quadrupole, respectively. The other symbols are explained in the text.

<i>L</i>	<i>l</i>	π	
1	0	—	<i>ED</i>
1	1	+	<i>MD</i>
2	1	+	<i>EQ</i>
2	2	—	<i>MQ</i>

one obtains

$$\mathbf{J}_{fi} = 4\pi \sum_{\mu=-1}^1 \hat{h}_{\mu} \sum_{l=0}^{\infty} i^l \times \sum_{m=-l}^l Y_l^m(\hat{k})^* (j_f m_f | Y_l^m(\hat{r}) j_l(kr) j^{\mu} | j_i m_i), \quad (3)$$

in which Y_l^m is the normalized spherical harmonic, and j_l is the spherical Bessel function. Then, using the fact that j^{μ} is a spherical component of a vector, hence transforms like Y_1^{μ} , a Clebsch-Gordan series for $Y_l^m(\hat{r}) j^{\mu}$ may be written:

$$Y_l^m(\hat{r}) j^{\mu} = \sum_{L,M} (LM | lm; 1\mu) \varphi_L^M, \quad (4)$$

in terms of a normalized set of tensors φ_L^M which transform under rotation like Y_L^M . If the Clebsch-Gordan coefficient in Eq. (4) is replaced by a Wigner $3j$ symbol¹¹ and the result substituted into Eq. (3), the resultant equation

$$\mathbf{J}_{fi} = -4\pi \sum_{\mu=-1}^1 \hat{h}_{\mu} \sum_{l=0}^{\infty} (-i)^l \sum_{m=-l}^l Y_l^m(\hat{k})^* \times \sum_{L,M} (-1)^M \begin{pmatrix} l & 1 & L \\ m & \mu & -M \end{pmatrix} (2L+1)^{\frac{1}{2}} \times (j_f m_f | j_l(kr) \varphi_L^M | j_i m_i) \quad (5)$$

is the basis for the multipole expansion. Since the nuclear radius is small compared to the wavelength of a γ ray, $kr \ll 1$, and since $j_l \sim (kr)^l$, the major contribution to the sum over l in Eq. (5) will come from the smallest value of l which can contribute. By Eq. (4), $l = L, L \pm 1$, and by Eq. (5), the minimum value of L is $|j_f - j_i|$ or 1, whichever is larger. (If one puts $L=0$ into Eq. (5), the resultant \mathbf{J}_{fi} will be parallel to \mathbf{k} ; hence $\hat{n} \cdot \mathbf{J}_{fi} = H_{fi} = 0$.) Therefore the smallest l is whichever of $l = |j_f - j_i|$, $||j_f - j_i| - 1|$ is allowed by parity conservation; according to Eq. (3), this requires $-(-1)^l = \pi_{fi}$. Table I gives the conventional nomenclature. Thus, for a given value of l , two values of L can contribute unless the smaller value is forbidden by the requirements $L \geq |j_f - j_i|$, $L > 0$, which is the case about half the time.

¹¹ A. R. Edmonds, *Angular Momentum in Quantum Mechanics* (Princeton University Press, Princeton, New Jersey, 1957), Chap. 3.

The Wigner-Eckart theorem,¹¹ applied to the nuclear matrix element of Eq. (5), says that

$$(j_f m_f | j_l(kr) \varphi_L^M | j_i m_i) = (-1)^{m_i} \begin{pmatrix} j_f & L & j_i \\ m_f & M & -m_i \end{pmatrix} \chi(L, l), \quad (6)$$

where χ is a reduced matrix element independent of m_f , and m_i . Then Eq. (5) can be rewritten

$$\mathbf{J}_{fi} = \sum_{L=l}^{l+1} \sum_{M,\mu,m} \begin{pmatrix} j_f & L & j_i \\ m_f & M & -m_i \end{pmatrix} \begin{pmatrix} l & 1 & L \\ m & \mu & -M \end{pmatrix} \times \hat{h}_{\mu} Y_l^{m*}(\hat{k}) \chi(L, l), \quad (7)$$

where we have absorbed certain irrelevant factors into χ .

3.2. Polarization and Absorption Probability

The complex polarization vector \hat{n} of the emitted radiation is that which maximizes $|\hat{n} \cdot \mathbf{J}_{fi}|^2$, subject to $\hat{n} \cdot \mathbf{k} = 0$. It is straightforward to show that

$$\hat{n} = \frac{\mathbf{J}^* - \hat{k}(\hat{k} \cdot \mathbf{J}^*)}{[|\mathbf{J}|^2 - |\hat{k} \cdot \mathbf{J}|^2]^{\frac{1}{2}}}, \quad (8)$$

and that the relative intensity I of the emitted radiation is

$$I = |\hat{n} \cdot \mathbf{J}|^2 = |\hat{k} \times \mathbf{J}|^2 = |\mathbf{J}|^2 - |\hat{k} \cdot \mathbf{J}|^2. \quad (9)$$

For the case of absorption, the analysis is changed only by the replacement of the emission term in Eq. (1) by its Hermitian conjugate. Therefore, the absorption probability is proportional to

$$\Sigma = |\hat{n}^* \cdot \mathbf{J}_{f'i'}|^2, \quad (10)$$

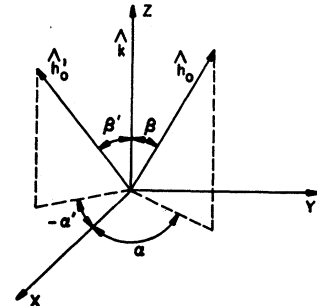
where $\mathbf{J}_{f'i'} = \mathbf{J}_{f'i}(-\hat{k}) = \mathbf{J}_{f'i}^*(\hat{k})$, and by using Eq. (8), it follows that

$$I\Sigma = |\mathbf{J}_{f'i'} \cdot \mathbf{J}_{fi}^* - (\hat{k} \cdot \mathbf{J}_{f'i'}) (\hat{k} \cdot \mathbf{J}_{fi}^*)|^2, \quad (11)$$

which gives the Mössbauer pattern for thin absorbers.

Since, in general, the magnetic fields have different directions in the emitter and absorber, the convenient quantization axes for the emitter \hat{h}_{μ} and for the absorber \hat{h}_{μ}' are different. It is desirable in the evaluation of Eqs. (9) and (11) to have all quantities expressed on the same basis. The most natural choice for the universal

FIG. 3. Euler angles, α , α' and β , β' , of the quantization axes \hat{h}_0, \hat{h}_0' for the emitter (unprimed) and absorber (primed). The third Euler angle, γ, γ' , is ignorable because it corresponds to a rotation of each system about its quantization axis. \hat{k} is the direction of propagation of the γ ray.



basis is one in which the z axis ($\boldsymbol{\eta}_0$) coincides with $\hat{\mathbf{k}}$. The remaining two basis vectors $\boldsymbol{\eta}_x, \boldsymbol{\eta}_y$ may be chosen arbitrarily, subject to the requirement that all three be mutually perpendicular.

Figure 3 shows the Euler angles $(\alpha, \beta, \gamma) \equiv \omega$ which are necessary to rotate $\boldsymbol{\eta}_\mu$ into $\hat{\mathbf{h}}_\mu$. The connection between $\boldsymbol{\eta}$ and $\hat{\mathbf{h}}$ is, in terms of the matrix elements of finite rotations $\mathcal{D}_{m'm}^{(L)}(\omega)$,¹¹

$$\hat{\mathbf{h}}_\mu = \sum_{\mu'} \mathcal{D}_{\mu'\mu}^{(1)}(\omega) \boldsymbol{\eta}_{\mu'}. \quad (12)$$

Similarly, rotating Y_l^m yields

$$\begin{aligned} Y_l^m(\hat{\mathbf{k}})^* &= \sum_{m'} \mathcal{D}_{m'm}^{(l)}(\omega) Y_l^{m'}(\boldsymbol{\eta}_0)^* \\ &= \left(\frac{2l+1}{4\pi} \right)^{\frac{1}{2}} \mathcal{D}_{0m}^{(l)}(\omega), \end{aligned} \quad (13)$$

and, upon substitution of Eqs. (12) and (13) into Eq. (7), the latter becomes

$$\begin{aligned} \mathbf{J}_{fi} &= \sum_{L=l}^{l+1} \sum_{M, m, \mu, \mu'} \begin{pmatrix} j_f & L & j_i \\ m_f & M & -m_i \end{pmatrix} \begin{pmatrix} l & 1 & L \\ m & \mu & -M \end{pmatrix} \\ &\quad \times \boldsymbol{\eta}_{\mu'} \mathcal{D}_{\mu'\mu}^{(1)}(\omega) \mathcal{D}_{0m}^{(l)}(\omega) \chi(L, l), \end{aligned} \quad (14)$$

which, by inserting the Clebsch-Gordan series for the product of \mathcal{D} functions,

$$\begin{aligned} \mathcal{D}_{\mu'\mu}^{(1)}(\omega) \mathcal{D}_{0m}^{(l)}(\omega) &= \sum_{JM'M''} (2J+1) \mathcal{D}_{M'M''}^{(J)*} \\ &\quad \times \begin{pmatrix} l & 1 & J \\ 0 & \mu' & M' \end{pmatrix} \begin{pmatrix} l & 1 & J \\ m & \mu & M'' \end{pmatrix}, \end{aligned} \quad (15)$$

and performing the sum over μ in Eq. (14),

$$(2J+1) \sum_{\mu} \begin{pmatrix} l & 1 & L \\ m & \mu & -M \end{pmatrix} \begin{pmatrix} l & 1 & J \\ m & \mu & M'' \end{pmatrix} = \delta_{M'', -M} \delta_{L, J}, \quad (16)$$

gives finally

$$\begin{aligned} \mathbf{J}_{fi} &= \sum_{L=l}^{l+1} \sum_{\mu} \begin{pmatrix} j_f & L & j_i \\ m_f & M & -m_i \end{pmatrix} \begin{pmatrix} l & 1 & L \\ 0 & \mu & -\mu \end{pmatrix} \\ &\quad \times \boldsymbol{\eta}_{\mu} (-1)^{\mu-M} \mathcal{D}_{\mu M}^{(L)}(\omega) \chi(L, l). \end{aligned} \quad (17)$$

A very similar expression obtains for $\mathbf{J}_{f'v'}$ if quantities appropriate to the absorber are substituted into Eq. (17).

If one defines a transverse matrix element of the current operator (proportional to the radiated electric field),

$$\boldsymbol{\varepsilon}_{fi} = \mathbf{J}_{fi} - \hat{\mathbf{k}}(\hat{\mathbf{k}} \cdot \mathbf{J}_{fi}), \quad (18)$$

then Eqs. (9) and (11) simplify to

$$I = |\boldsymbol{\varepsilon}_{fi}|^2, \quad (9')$$

$$I\Sigma = |\boldsymbol{\varepsilon}_{f'v'} \cdot \boldsymbol{\varepsilon}_{fi}^*|^2. \quad (11')$$

If the sums over μ and L are written out, the magnetic and electric components may be identified:

$$\begin{aligned} \boldsymbol{\varepsilon}_{fi} &= \begin{pmatrix} j_f & l+1 & j_i \\ m_f & M & -m_i \end{pmatrix} \chi(E2^{l+1}) \\ &\quad \times (\boldsymbol{\eta}_1 \mathcal{D}_{1M}^{(l+1)}(\omega) + \boldsymbol{\eta}_{-1} \mathcal{D}_{-1M}^{(l+1)}(\omega)) \\ &\quad + \begin{pmatrix} j_f & l & j_i \\ m_f & M & -m_i \end{pmatrix} \chi(M2^l) \\ &\quad \times (\boldsymbol{\eta}_1 \mathcal{D}_{1M}^{(l)}(\omega) - \boldsymbol{\eta}_{-1} \mathcal{D}_{-1M}^{(l)}(\omega)). \end{aligned} \quad (19)$$

Here some more irrelevant factors have been absorbed into the reduced nuclear matrix elements χ .

From Eq. (19), we can calculate I and $I\Sigma$. Substituting for \mathcal{D} according to

$$\mathcal{D}_{m'm}^{(j)}(\alpha\beta\gamma) = e^{im'\alpha} d_{m'm}^{(j)}(\beta) e^{im\gamma}, \quad (20)$$

where d is real, we get

$$\begin{aligned} I &= \begin{pmatrix} j_f & l+1 & j_i \\ m_f & M & -m_i \end{pmatrix}^2 |\chi(E2^{l+1})|^2 \\ &\quad \times \{ (d_{1M}^{(l+1)})^2 + (d_{-1M}^{(l+1)})^2 \} \\ &\quad + \begin{pmatrix} j_f & l & j_i \\ m_f & M & -m_i \end{pmatrix}^2 |\chi(M2^l)|^2 \\ &\quad \times \{ (d_{1M}^{(l)})^2 + (d_{-1M}^{(l)})^2 \} \\ &\quad + 2 \begin{pmatrix} j_f & l+1 & j_i \\ m_f & M & -m_i \end{pmatrix} \begin{pmatrix} j_f & l & j_i \\ m_f & M & -m_i \end{pmatrix} \\ &\quad \times \text{Re}[\chi(E2^{l+1})\chi(M2^l)] \\ &\quad \times \{ d_{1M}^{(l+1)} d_{1M}^{(l)} - d_{-1M}^{(l+1)} d_{-1M}^{(l)} \}, \end{aligned} \quad (21)$$

which is the general intensity distribution for a multipole mixture, consisting of an electric term, a magnetic term, plus an interference term. Equation (21) can be reduced to a sum over Legendre polynomials and a similar expression (albeit a much more complicated function, not only of β , but also of β' and $|\alpha - \alpha'|$) written down for $I\Sigma$.

For the sake of clarity and simplicity, we shall for the moment restrict ourselves to pure multipole emission. In that case, the formulas are simpler:

$$I = \begin{pmatrix} j_f & L & j_i \\ m_f & M & -m_i \end{pmatrix}^2 \{ d_+^2 + d_-^2 \} \quad (22)$$

$$\begin{aligned} I\Sigma &= \begin{pmatrix} j_f & L & j_i \\ m_f & M & -m_i \end{pmatrix}^2 \begin{pmatrix} j_{f'} & L & j_{i'} \\ -m_{f'} & M & m_{i'} \end{pmatrix}^2 \\ &\quad \times \{ d_+^2 d_+'^2 + d_-^2 d_-'^2 + 2 \cos(\alpha - \alpha') d_+ d_+ d_+' d_-' \}. \end{aligned} \quad (23)$$

It is now relatively easy to evaluate the angular dependence of the Mössbauer pattern. The d functions

TABLE II. Reduced rotation matrix elements, $d_{\mu M}^{(L)}$, for dipole and quadrupole cases.

μ	M	$d_{\mu M}^{(1)}$	$d_{\mu M}^{(2)}$
± 1	± 2	...	$\mp(2 \sin \beta + \sin 2\beta)/4$
± 1	± 1	$\cos^2(\beta/2)$	$(\cos \beta + \cos 2\beta)/2$
± 1	0	$\pm(1/\sqrt{2}) \sin \beta$	$\pm(3/8)^{1/2} \sin 2\beta$
± 1	∓ 1	$\sin^2(\beta/2)$	$(\cos \beta - \cos 2\beta)/2$
± 1	∓ 2	...	$\pm(2 \sin \beta - \sin 2\beta)/4$

can be calculated from prescriptions given by Edmonds; they are tabulated in Table II for the dipole and quadrupole cases, and the angular distributions I are given in Table III.

In the evaluation of $I\Sigma$, it is convenient to use a different approach. One can see from Eq. (11') that $I\Sigma$ is the square of the magnitude of the inner product of two complex vectors. It should therefore be possible to express it in the form

$$I\Sigma = II' \cos^2 \Theta, \quad (24)$$

where Θ is the "angle" between the two complex vectors $\mathbf{\epsilon}^*$ and $\mathbf{\epsilon}'$. One could then factor out I and get the cross section by itself, which is necessary for thick absorber calculations.

3.3. Complex Vector Parameterization

The vectors in which we are interested are the two-dimensional complex vectors $\mathbf{\epsilon}$. To specify one of them, four parameters are necessary; for example, the real and imaginary parts of each of the components. It is the purpose of this section to find a more convenient parameterization.

We consider a vector \mathbf{A} :

$$\begin{aligned} \mathbf{A} &= a_x \hat{i} + a_y \hat{j} = a_+ \boldsymbol{\eta}_+ + a_- \boldsymbol{\eta}_- \\ \boldsymbol{\eta}_{\pm} &= \mp (\hat{i} \pm i \hat{j}) / \sqrt{2} \\ a_{\pm} &= \mp (a_x \mp i a_y) / \sqrt{2}, \end{aligned} \quad (25)$$

and rotate it through an angle φ , simultaneously multiplying it by an over-all phase factor. Symbolically,

$$\mathbf{A} = R \mathbf{A}', \quad (26)$$

where R is the rotation operator times $e^{i\delta}$. By the proper choice of φ and δ , it is always possible to obtain, for any \mathbf{A} ,

$$\mathbf{A}' = A_x \hat{i} + i A_y \hat{j}, \quad (27)$$

 TABLE III. Angular distribution for dipole and quadrupole radiation. $\mathcal{G}_m^{L \equiv I} = \left(\frac{j_f}{m_f} \quad L \quad j_i}{M \quad -m_i} \right)^2$.

M	\mathcal{G}_M^1	\mathcal{G}_M^2
± 2	...	$(4 \sin^2 \beta + \sin^2 2\beta)/8$
± 1	$(1 + \cos^2 \beta)/2$	$(\cos^2 \beta + \cos^2 2\beta)/2$
0	$\sin^2 \beta$	$\frac{3}{4} \sin^2 2\beta$

where A_x and A_y are both real. We now define an angle ξ ;

$$\begin{aligned} A_x &= A \cos \xi \\ A_y &= A \sin \xi, \end{aligned} \quad (28)$$

where $A^2 = A_x^2 + A_y^2 = |\mathbf{A}|^2$. $|\tan \xi|$ is therefore the ratio of the axes of the polarization ellipse. The spherical components transform according to

$$\begin{aligned} e^{-i\delta} a_{\pm} &= e^{\pm i\varphi} a'_{\pm} = \mp [(A_x \pm A_y) / \sqrt{2}] e^{\pm i\varphi}, \\ &= \mp A e^{\pm i\varphi} (\cos \xi \pm \sin \xi) / \sqrt{2}. \end{aligned} \quad (29)$$

Any two-dimensional complex vector is then specified by four real numbers; its length A , its elliptical eccentricity parameter ξ , the angle φ by which the axes of the ellipse differ from the x, y axes, and the over-all phase δ . One can see from Eq. (29) that

$$\tan \xi = \frac{e^{-i\delta} a_+ + e^{i\delta} a_-^*}{e^{-i\delta} a_+ - e^{i\delta} a_-^*}. \quad (30)$$

The inner product of two vectors \mathbf{A} and \mathbf{B} is

$$\begin{aligned} \mathbf{A}^*(A, \xi, a, \delta) \cdot \mathbf{B}(B, \eta, b, \epsilon) &= AB e^{i(\epsilon - \delta)} \{ \cos(a - b) \cos(\xi - \eta) \\ &\quad - i \sin(a - b) \sin(\xi + \eta) \}, \end{aligned} \quad (31)$$

which can be shown to be

$$\mathbf{A}^* \cdot \mathbf{B} = AB \cos \Theta e^{i(\psi + \epsilon - \delta)}, \quad (32)$$

where

$$\psi = -\arctan \{ \tan(a - b) \sin(\xi + \eta) / \cos(\xi - \eta) \}, \quad (33)$$

and where 2Θ is the angle between $(2\xi, 2a)$ and $(2\eta, 2b)$ when they are polar and azimuthal angles as shown in Fig. 4. This accomplishes the aim expressed in Eq. (24).

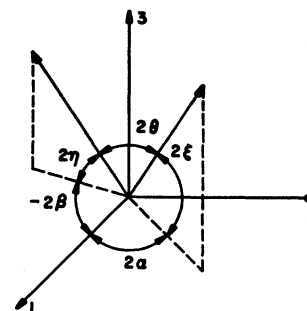


FIG. 4. Relation between the angle Θ between two complex vectors and their eccentricity angles ξ, η and their azimuths α, β .

3.4. Application to Pure Multipole Case

The electric vectors $\mathbf{\epsilon}$ for pure multipole fields can be seen from Eq. (19) and Eq. (20) to have $\varphi = \alpha$ and $\delta = M\gamma$ plus the phase of the reduced nuclear matrix element χ . To wit, for $M2^l$,

$$\mathbf{\epsilon}_{fi} = \begin{pmatrix} j_f & l & j_i \\ m_f & M & -m_i \end{pmatrix} \chi \mathbf{E}, \quad (34)$$

$$\mathbf{E} = e^{iM\gamma} (\boldsymbol{\eta}_+ e^{i\alpha} d_{1M}^{(l)}(\beta) - \boldsymbol{\eta}_- e^{-i\alpha} d_{-1M}^{(l)}(\beta)).$$

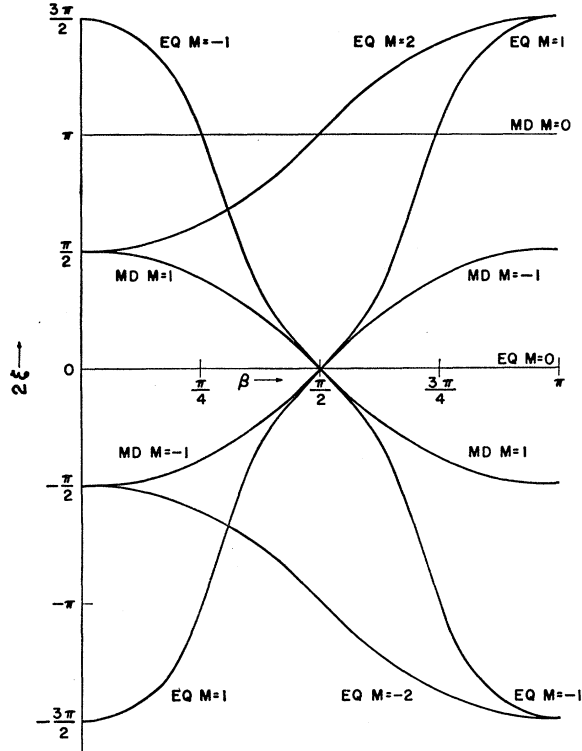


Fig. 5. Eccentricity angle ξ plotted as a function of polar angle β for $M1$ and $E2$ radiation. Circular polarization corresponds to an odd multiple of $\pi/4$, linear polarization to a multiple of $\pi/2$, and intermediate values to elliptical polarization of varying eccentricity.

For $E2^{l+1}$, one replaces l by $l+1$ and changes the sign of η_- .

By inspection of Eq. (34), Table II, and Eq. (30), $\tan\xi$ may be deduced. It is given in Table IV. The other entries in Table IV, $\cos 2\xi$ and $\sin 2\xi$, are there because $I\Sigma$, Eq. (11') is of the form

M	$\tan\xi$	$\cos 2\xi$	$\sin 2\xi$
(a) Magnetic dipole			
± 1	$\pm \cos\beta$	$\frac{\sin^2\beta}{1+\cos^2\beta}$	$\frac{\pm 2 \cos\beta}{1+\cos^2\beta}$
0	∞	-1	0
(b) Electric quadrupole			
± 2	$\pm \frac{1}{\cos\beta}$	$\frac{\sin^2\beta}{1+\cos^2\beta}$	$\frac{\pm 2 \cos\beta}{1+\cos^2\beta}$
± 1	$\pm \frac{\cos\beta}{\cos 2\beta}$	$\frac{\cos^2 2\beta - \cos^2\beta}{\cos^2 2\beta + \cos^2\beta}$	$\frac{\pm 2 \cos\beta \cos 2\beta}{\cos^2 2\beta + \cos^2\beta}$
0	0	1	0

$$I\Sigma = \frac{1}{2}I(\beta)I'(\beta')\{1 + \sin 2\xi \sin 2\xi' + \cos 2\xi \cos 2\xi' \cos 2(\alpha - \alpha')\} \\ = \frac{1}{2}I(\beta)I'(\beta')\{1 + \cos 2\Theta\} = I(\beta)I'(\beta') \cos^2\Theta. \quad (35)$$

To facilitate the use of Eq. (35), we have plotted ξ as a function of β for the cases given in Table IV. These graphical solutions are shown on Fig. 5. By use of

Eq. (35) and Table IV, we can also calculate $\cos^2\Theta$. This is given in Table V, which is valid for both magnetic and electric radiation. The missing entries can be filled in by using the symmetry property $\cos^2\Theta(\beta, \beta')_{MM'} = \cos^2\Theta(\beta', \beta)_{M'M}$.

In summary, then, the intensity of a given line is proportional to

$$I = \begin{pmatrix} j_f & L & j_i \\ m_f & M & -m_i \end{pmatrix}^2 g_{M^L}(\beta), \quad (36)$$

where $g_{M^L}(\beta)$ is given in Table III for $L=1, 2$. The absorption cross section is proportional to

$$\Sigma = I'(\beta') \cos^2\Theta \\ = \begin{pmatrix} j_f' & L & j_i' \\ -m_f' & M' & m_i' \end{pmatrix}^2 g_{M'^L}(\beta') \cos^2\Theta, \quad (37)$$

where $\cos^2\Theta$ can be obtained either exactly from Table V or approximately from Figs. 4 and 5. The $3j$ symbols must be calculated for each case; for Fe^{57} ($j_f = \frac{1}{2}$, $j_i = \frac{3}{2}$, $L=1$), they are given in Table VI.

3.5. Multipole Mixtures

More complicated is the situation when both $E2^{l+1}$ and $M2^l$ radiations contribute to the same transition. Then the electric field vector has the form

$$\mathbf{E}_{fi} = a\mathbf{E}_M^{l+1} + b e^{i\varphi} \mathbf{E}_{M'}^l, \quad (38)$$

where a and $b e^{i\varphi}$ are products of the appropriate Wigner $3j$ symbols and reduced matrix elements $\chi(L, l)$. We can choose a, b to be real; the relative phase of the nuclear matrix elements is then φ . The intensity I can easily be calculated from Eq. (38); it is

$$I = |\mathbf{E}_{fi}|^2 = a^2 g_{M^{l+1}} + b^2 g_{M'^l} \\ + 2ab (g_{M^{l+1}} g_{M'^l})^{1/2} \cos\varphi \cos(\xi_{M'}^l - \xi_{M^{l+1}}). \quad (39)$$

Not so easily found, however, is $I\Sigma$ in this case. In order to accomplish our aim of factoring out the incident intensity from $I\Sigma$ to get the absorption cross section, we must consider the problem of obtaining the polarization parameters of the sum of two complex vectors.

Our task is to find the length C , eccentricity angle μ , and polarization azimuth γ of

$$\mathbf{C}(C, \mu, \gamma) e^{i\psi} = \mathbf{A}(A, \xi, \alpha) + e^{i\varphi} \mathbf{B}(B, \eta, \alpha), \quad (40)$$

the sum of two vectors of the form of Eq. (38), where the azimuth α is the same in both terms on the right.

TABLE V. Fractional overlap cos²Θ for dipole and quadrupole radiation.

<i>M</i>	<i>M'</i>	cos ² Θ
(a) Dipole radiation		
1 -1	$\frac{\pm 1}{\mp 1}$	$\frac{(\cos\beta \pm \cos\beta')^2 + \sin^2\beta \sin^2\beta' \cos^2(\alpha - \alpha')}{(1 + \cos^2\beta)(1 + \cos^2\beta')}$
±1	0	$\frac{1 - \sin^2\beta \cos^2(\alpha - \alpha')}{1 + \cos^2\beta}$
0	0	cos ² (α - α')
(b) Quadrupole radiation		
2 -2	$\frac{\pm 2}{\mp 2}$	Same as for dipole (1, ±1)
2 -2	$\frac{\pm 1}{\mp 1}$	$\frac{(\cos 2\beta' \pm \cos\beta \cos\beta')^2 - \cos^2(\alpha - \alpha') \sin^2\beta (\cos^2 2\beta' - \cos^2\beta')}{(\cos^2 2\beta' + \cos^2\beta')(1 + \cos^2\beta)}$
±2	0	Same as for dipole (±1, 0)
1 -1	$\frac{\pm 1}{\mp 1}$	$\frac{(\cos\beta' \cos 2\beta \pm \cos\beta \cos 2\beta')^2 + \cos^2(\alpha - \alpha') (\cos^2 2\beta - \cos^2\beta) (\cos^2 2\beta' - \cos^2\beta')}{(\cos^2 2\beta + \cos^2\beta) (\cos^2 2\beta' + \cos^2\beta')}$
±1	0	$\frac{\cos^2\beta \sin^2(\alpha - \alpha') + \cos^2(\alpha - \alpha') \cos^2 2\beta}{(\cos^2 2\beta + \cos^2\beta)}$
0	0	Same as for dipole (0,0)

We have chosen the over-all phase (δ, Sec. 3.3) to be zero for **A**, φ for **B**. Writing out the vectors in the form

$$\mathbf{A} = a_+ \boldsymbol{\eta}_+ e^{i\alpha} + a_- \boldsymbol{\eta}_- e^{-i\alpha}, \tag{41}$$

and using relations like

$$\begin{aligned} a_+ &= A \cos(\xi - \frac{1}{4}\pi), \\ a_- &= A \sin(\xi - \frac{1}{4}\pi), \end{aligned} \tag{42}$$

which follow from Eq. (30), it is straightforward to solve for γ and μ in Eq. (40). First we write

$$\frac{C_+}{C_-} e^{2i(\gamma - \alpha)} = \frac{a_+ + e^{i\varphi} b_+}{a_- + e^{i\varphi} b_-}; \tag{43}$$

then take real and imaginary parts of both sides, yielding

$$\cot(\mu - \frac{1}{4}\pi) \sin 2(\gamma - \alpha) = \frac{2AB \sin \varphi \sin(\xi - \eta)}{A^2(1 - \sin 2\xi) + B^2(1 - \sin 2\eta) + 2AB \cos \varphi [\cos(\xi - \eta) - \sin(\xi + \eta)]}, \tag{44}$$

$$\cot(\mu - \frac{1}{4}\pi) \cos 2(\gamma - \alpha) = \frac{-A^2 \cos 2\xi - B^2 \cos 2\eta - 2AB \cos \varphi \cos(\xi + \eta)}{A^2(1 - \sin 2\xi) + B^2(1 - \sin 2\eta) + 2AB \cos \varphi [\cos(\xi - \eta) - \sin(\xi + \eta)]}, \tag{45}$$

The ratio of Eqs. (44) and (45) give γ - α, after which μ may be found with Eq. (44). The magnitude C is given by [compare Eq. (39)]

$$C^2 = A^2 + B^2 + 2AB \cos \varphi \cos(\xi - \eta). \tag{46}$$

We have not found a way to significantly simplify Eqs. (44) and (45) for the case where A and B have comparable magnitudes, but it is often true that one multipole contribution is dominant, say **A**. Then, if terms of order B²/A² and higher are neglected, Eqs. (44) and (45) can be manipulated to give

$$\mu - \xi = -r \cos \varphi \sin(\xi - \eta), \tag{47}$$

$$\gamma - \alpha = -r [\sin \varphi \sin(\xi - \eta) / \cos 2\xi], \tag{48}$$

where r = B/A. Equation (48) obviously breaks down when ξ = ±π/4, ±3π/4; this is because the polarization angle of a circularly polarized wave is undefined.

The effect on the product, |**A***·**A**'|², of adding to **A** a small **B**e^{iφ} and to **A**' a small **B**'e^{iφ'} can be broken up into three parts, according to Eq. (32); A² and A'² are

TABLE VI. Wigner 3j symbols for Fe⁵⁷: $\begin{pmatrix} \frac{1}{2} & 1 & \frac{3}{2} \\ m_f & M & -m_i \end{pmatrix}$.

<i>m_f</i> \ <i>m_i</i>	$\frac{3}{2}$	$\frac{1}{2}$	$-\frac{1}{2}$	$-\frac{3}{2}$
$\frac{1}{2}$	$-\frac{1}{2}$	$\sqrt{1/6}$	$-\sqrt{1/12}$	0
$-\frac{1}{2}$	0	$\sqrt{1/12}$	$-\sqrt{1/6}$	$\frac{1}{2}$

changed according to Eq. (46), and $\cos^2\Theta$ becomes

$$\cos^2\Theta \rightarrow \cos^2\Theta + r \sin(\xi - \eta) \{ \sin\varphi \cos 2\xi' \sin 2(\alpha - \alpha') - \cos\varphi [\cos 2\xi \sin 2\xi' - \sin 2\xi \cos 2\xi' \cos 2(\alpha - \alpha')] \}, \quad (49)$$

plus another term with primed quantities exchanged for unprimed ones, and vice versa. (Except for φ , since we are dealing with the same two nuclear states in the emitter and absorber, the relative phases of multipoles are the same.)

3.6. Application of the Formalism

In order to calculate shapes of Mössbauer lines, we must know the proportionality factor K between the actual cross section at resonance σ_r and Σ , Eq. (37).

$$\sigma_r = \sum_{m_i m_f'} K \Sigma, \quad (50)$$

where the sum is over all pairs of substates which contribute to the resonance. K is most easily evaluated by considering the special case of no splitting in the absorber. Then we know that whatever is the polarization of the incident beam,

$$\sigma_0 = 2\pi\lambda^2 \frac{2j_f + 1}{2j_i + 1} \frac{f'}{1 + \alpha}, \quad (51)$$

where α is the internal conversion coefficient and f' is the Debye-Waller factor for the absorber. By putting $\beta = \beta' = 0$ in the formulas for ϑ and $\cos^2\Theta$ [Eqs. (22) and (35)], one finds $K = (2L + 1)\sigma_0$.

If a gamma-ray beam of Lorentzian energy distribution is incident on a resonant absorber, the transmitted beam has a shape proportional to

$$P(x, t) = \frac{\Gamma}{2\pi} \int_0^\infty \frac{dE}{(E - E_0 + S)^2 + \Gamma^2/4} \times \exp\left(-t \frac{\Gamma/4}{(E - E_0)^2 + \Gamma^2/4}\right), \quad (52)$$

where Γ is the natural width of both the incident beam and the resonant absorber, E_0 is the resonance energy, and S is the Doppler shift of the incident beam.¹² The normalization factor has been chosen so that P is a function only of $x = S/\Gamma$ and $t = n\sigma_r$.

By expanding the exponential in the integrand of P and evaluating each term in the resultant sum by contour integration, it is relatively straightforward to show that, for $E_0 \gg \Gamma$

¹² If the source is thick and is resonant absorbing, the beam incident on the absorber will not be Lorentzian with the natural width. Calculations of the transmission integral for that case as well have been performed by S. Margulies and J. R. Ehrman, Nuclear Instruments and Methods **12**, 131 (1961).

$$P = e^{-(t/4) \sin^2 \varphi} \cos\left(\frac{t \sin^3 \varphi}{\cos \varphi}\right) - \sum_{\mu=1}^\infty e^{-t/2} I_\mu(t/2) \cos(\mu\varphi) (\cos^{-\mu}\varphi - \cos^\mu\varphi), \quad (53)$$

where $\varphi = \arcsin(1 + x^2)^{-1/2}$, and I_μ is the Bessel function of order μ and imaginary argument.

It can be shown, using either Eq. (53) or (52), that

$$\lim_{x \rightarrow 0} P(x, t) = e^{-t/2} I_0(t/2) \quad (54)$$

$$P(x, t) = 1 - \frac{t/2}{1 + x^2} + \dots \quad t \ll 1.$$

We have evaluated $P(x, t)$ in the form given by Eq. (53) on the IBM 704. The result is that, to about $\frac{1}{2}\%$, it is given by

$$1 - P(x, t) = [1 - P(0, t)] \bar{\Gamma}^2 / (S^2 + \bar{\Gamma}^2), \quad (55)$$

where

$$\begin{aligned} \bar{\Gamma}/\Gamma &= 1.00 + 0.135t & 0 \leq t \lesssim 5 \\ &= 1.01 + 0.145t - 0.0025t^2 & \text{for } 4 \lesssim t \lesssim 10. \end{aligned} \quad (56)$$

To a good approximation, then, the shape and intensity of a Mössbauer absorption line is

$$A(S) = fI(\beta) (1 - P(0, t)) \bar{\Gamma}^2 / (S^2 + \bar{\Gamma}^2), \quad (57)$$

where f is the Debye-Waller factor for the source and t is calculated from Eq. (50) without the sum, of course, if the absorber lines are split more than their width; with it if they are unsplit. In the intermediate case (overlapping absorber lines), Eq. (52) is no longer applicable.

As an example, we will evaluate Eq. (57) for the 10.65-mm/sec line in Fe⁵⁷. This line is formed by the overlap of the $\frac{3}{2} \rightarrow \frac{1}{2}$ source line with the $-\frac{1}{2} \rightarrow -\frac{3}{2}$ absorber line. We shall take an absorber thickness of 1.75 mg/cm² of Fe⁵⁷; for angles, we take $\beta = 30^\circ$, $\beta' = 60^\circ$, $\alpha - \alpha' = 90^\circ$. The effective absorber thickness is $1.75/\sin 60^\circ = 2.01$ mg/cm² which corresponds to $n = 21.2 \times 10^{18}$ atoms/cm². σ_0 for Fe⁵⁷ is 1.48×10^5 b. From Table VI, we find that the square of the $3j$ symbol is $\frac{1}{4}$ for both source and absorber, and Table III then says $I(30^\circ) = \frac{7}{32}$, $I'(60^\circ) = \frac{5}{32}$. $\cos^2\Theta$ may be evaluated from Table V(a), in which M, M' are always the difference between excited and ground state m 's. The result is $\cos^2\Theta = 8(2 - \sqrt{3})/35$. Then Eq. (37) gives $\Sigma = \frac{5}{32} \cos^2\Theta = 9.57 \times 10^{-3}$; hence $t = 0.0830$ if we take $f' = 0.922$. For this line, then, we have a very thin absorber, and we can use Eq. (54) to find $1 - P(0, t) = 0.0415$. Equation (56) gives $\bar{\Gamma} = 1.01\Gamma$ which determines the effective width of the line, and finally Eq. (57), with $f = 0.916$, yields $A(0) = 0.0083$. This should be the relative absorption strength at the 10.65-mm/sec line.

An alternative way to determine Θ is first to find 2ξ and $2\xi'$ either from Table IV or Fig. 5 and use the fact

that 2Θ is the angle between the vectors $(2\xi, 2\alpha)$ and $(2\xi', 2\alpha')$ as shown on Fig. 4 or in Eq. (35).

Because it becomes rather tedious to calculate these absorptions when one has many lines, we have programmed the Fe^{57} problem for the IBM 704. Figure 6 shows some of the results of this machine calculation with all parameters except angles the same as those used in the above example. An extensive compilation of these graphs is in preparation.¹³

To take into account the possibility of nuclear alignment, one need only insert weighting factors for the initial states of source and absorber nuclei into Eq. (22). The *average* of the weighting factors should be unity, their sum $2j_i+1$, $2j_i'+1$ for source and absorber, respectively.

The modifications which are necessary in the above procedure to extend it to multipole mixtures are straightforward. First, instead of having ${}^m K$, Eq. (50), equal to $(2L+1)\sigma_0$, it is now

$$K = \sigma_0 \left[\frac{|\chi(E2^{l+1})|^2}{2l+3} + \frac{|\chi(M2^l)|^2}{2l+1} \right]^{-1}, \quad (58)$$

which follows from Eq. (21). The absorption is determined in a way analogous to the pure multipole case. I is found from Eq. (39), and $\cos^2\Theta$ by solving Eqs. (44) and (45), in which A and B are to be set equal to the appropriate $3j$ symbols times \sqrt{g} times the absolute value of χ . In the case that one of the nuclear matrix elements is much smaller than the other, $\cos^2\Theta$ may more easily be found from Eq. (49). Since in the case of multipole mixtures, there are two parameters, the relative strength and the phase of the multipole components, which are usually not well known experimentally, the fitting of a Mössbauer absorption pattern which involves mixtures is considerably more difficult than the pure multipole case.

4. EXPERIMENTAL ARRANGEMENTS

4.1. A Simple Experiment

Before discussing experimental problems, a description of an extremely simple setup will show the ease with which the elliptical polarization can be demonstrated. Source and absorber consist of iron metal. Both are placed in solenoids, as shown in Fig. 6. If the fields in the two solenoids are parallel, the absorption at the central peak, i.e., at zero relative velocity between source and absorber, is very much larger than that for antiparallel fields. A glance at Figs. 1 and 2 shows why; at $\theta=20^\circ$, the emitted and absorbed photons are already nearly circularly polarized. In parallel fields, right-circularly-polarized photons fit into "right-circularly-polarized" absorption levels. In antiparallel fields, the polarization of the emission components does not

¹³ W. M. Visscher (unpublished).

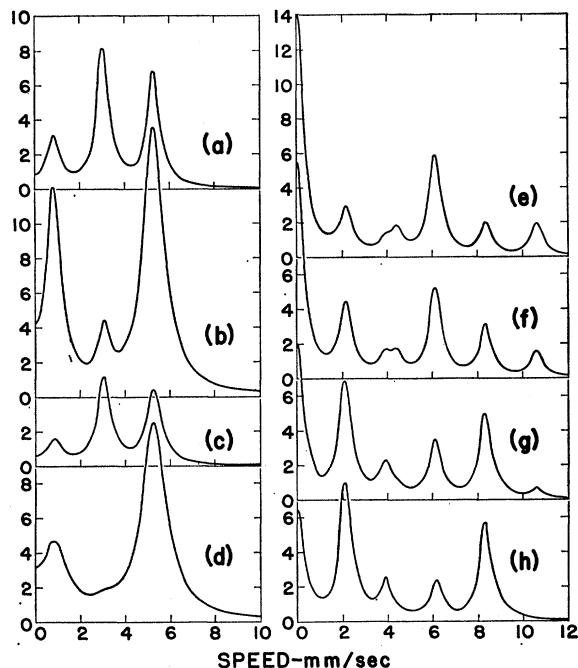


Fig. 6. Calculated absorption curves for Fe^{57} . Absorber thickness is 1.75 mg/cm^2 Fe^{57} , the natural width is taken to be 0.3 mm/sec , f and f' are 91.6 and 92.2% , respectively. Positive Doppler shifts (abscissa) only are shown; the patterns are symmetrical. Curves (a) and (b) are for an unsplit source and the absorber at 90° and 15° to the beam. Notice the marked broadening of the intense lines for $\beta'=15^\circ$ due to the effectively very thick absorber. Curves (c) and (d) are the same but for source split and parallel to the absorber, which is unsplit. Curves (e), (f), (g), and (h) are for both source and absorber split and inclined 60° to the beam with azimuthal angles of $0, 30, 60,$ and 90° , respectively. Ordinates are all to the same arbitrary scale.

fit those of the absorption components, and the absorption at zero velocity is small.

4.2. Experimental Procedure

The simple arrangement shown in Fig. 7 and discussed in Sec. 4.1 demonstrates the helicity of the individual Zeeman components quite easily. For a detailed comparison between theory and experiment, a somewhat more refined arrangement is required. Even though the basic ideas are extremely simple, some unexpected problems turned up, particularly connected with the magnetization of very thin iron foils. These problems will be discussed briefly in the next section.

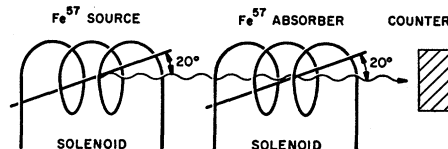


Fig. 7. A simple experiment to demonstrate the circular polarization of the 14.4-keV gamma rays from Fe^{57} . The counting rate with parallel fields is much larger than with antiparallel fields at source and absorber.

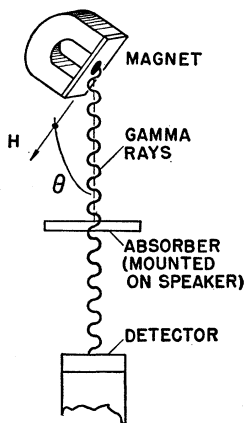


FIG. 8. Arrangement to measure the angular dependence of the Zeeman components of a "six-line source." (Experiment I in text.)

In order to get complete information, Mössbauer spectra were recorded for various source and absorber combinations and for a number of angles between external magnetic field and source and/or absorber. The source-absorber combinations which provided the essential information are shown in Table VII.

TABLE VII. Source-absorber combinations.

Experiment	Source	Absorber
I. Six-line source, single-line absorber	10-mC Co ⁵⁷ , coplated with Fe ⁵⁶ , diffused into a 20-mil natural iron foil	0.56-mg/cm ² Fe, 75% Fe ⁵⁷ diffused into 3.5-mg/cm ² Ti
II. Single-line source six-line absorber	Co ⁵⁷ in Co (8%) Pd alloy	4.5-mg/cm ² natural Fe foil (2.2% Fe ⁵⁷)
III. Six-line source six-line absorber	10-mC Co ⁵⁷ , diffused into natural iron foil	2.3-mg/cm ² Fe, 75% enriched in Fe ⁵⁷

For the measurement of the spectra, either source or absorber was mounted on a Jensen 8-in. Flexair woofer and moved sinusoidally at a frequency of 11 sec⁻¹. The output pulses from a scintillation counter were energy selected by a single-channel analyzer and modulated with a saw tooth voltage, which was locked in with the speaker drive. The modulated pulses were displayed on a 400-channel RIDL analyzer and thus yielded directly

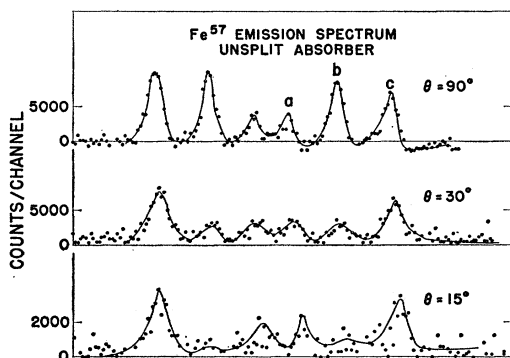


FIG. 9. Zeeman spectrum of six-line source, measured at three angles θ with a single-line absorber. (Experiment I in text.)

the desired Mössbauer spectrum,¹⁴ as shown in Figs. 7 to 9. Due to the sinusoidal drive and linear display, the velocity scale in these figures is sinusoidal. The slight drop to the right in each spectrum is caused by the dead-time effect in the 400-channel analyzer.

For experiment I, the source was fixed to a magnet, as shown in Fig. 8. For experiment II, the absorber was placed between two Styrofoam plates and mounted between slender polepieces in such a way that the magnetic field was in the plane of the absorber, and the gamma rays could pass through the absorber at angles between 20° and 90° to the magnetic field. For experiment III, both source and absorber were placed in magnetic fields.

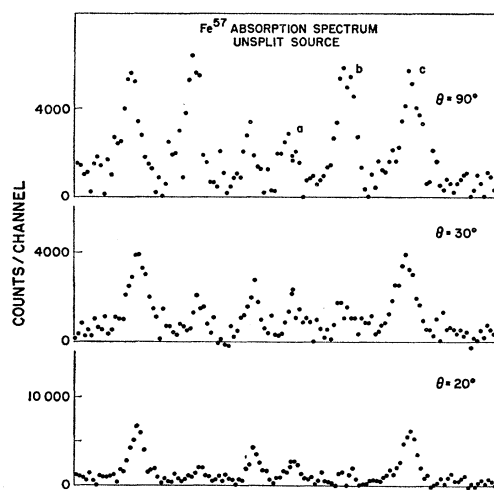


FIG. 10. Absorption of a single-line spectrum by a six-line absorber as a function of the angle θ between incoming gamma ray and magnetic field. (Experiment II.)

5. RESULTS AND DISCUSSION

5.1. Results

Typical results are shown in Figs. 9, 10, and 11. The intensities in Fig. 9 and Fig. 10 can be compared directly with the predictions displayed in Fig. 2. The agreement is satisfactory. In particular, one can see that the $\Delta m=0$ lines disappear as one approaches the longitudinal case, but that they are strongest in the transverse Zeeman case.

Figure 11, which represents an experiment of type III, should be compared with Fig. 12, the result of an IBM 704 calculation. Here again one can see the helicity of the various components rather directly.

The experimental problems encountered in the present experiment are all rather straightforward with one exception. Superficially, experiment I and experiment II of Sec. 4 look very similar. Experimentally,

¹⁴ S. L. Ruby, L. M. Epstein, and K. H. Sun, Rev. Sci. Instr. **31**, 580 (1960).

however, they are quite different. It is easy to get the correct intensity ratios in experiments of type I. Close to the direction of the magnetic field, the intensities of the six lines are $3:\epsilon:1:1:\epsilon:3$, where ϵ is very small. No matter how thick the absorber, the very weak line cannot be enhanced relative to the other lines. In an experiment of type II, all incoming components have the same energy. If the absorber is very thick, the absorption component will saturate, and one will find an appreciable absorption component $\Delta m=0$ even close to $\theta=0^\circ$. Indeed, all the early experiments showed a ratio of about $3:4:1$ rather than the expected $3:\epsilon:1$. Reducing the absorber thickness from 3 to 1.73 mg/cm^2 enriched iron did, however, not quench the $\Delta m=0$ lines. It turned out that this foil, while still quite thick for the gamma rays, was magnetically too thin. The typical thicknesses for domains in iron are about 10μ . The $2\text{-}\mu$ foil was apparently not magnetized in the plane of the foil. In order to check this assumption, natural foils of 4.5 mg/cm^2 (about 6μ) thickness were used. The results with these foils show the expected behavior and the expected decrease in the $\Delta m=0$ component as displayed by Fig. 10.

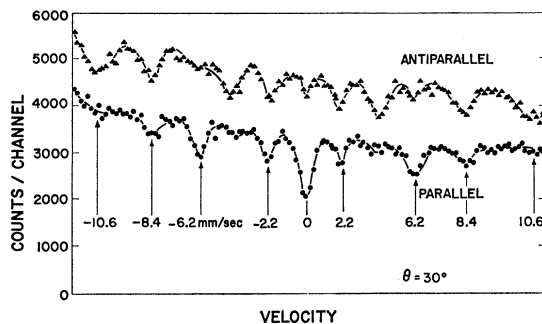


FIG. 11. Six-line source and six-line absorber. Emitted and absorbed gamma rays each subtend angles of 30° with the magnetic fields at the source and the absorber, respectively. Parallel and antiparallel labels on the curves refer to magnetic field directions in source and in absorber. The two curves in this figure should be compared with the curves calculated from the theory in Sec. 3 and displayed in Fig. 12.

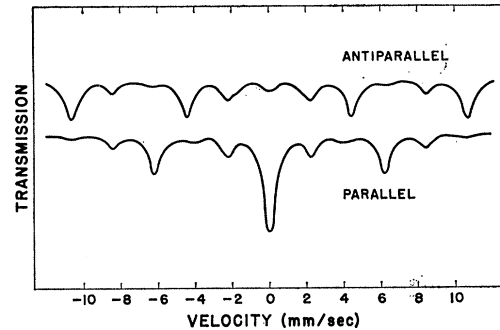


FIG. 12. Calculated absorption spectra for the parameters of experiment III in text. The natural width Γ is taken to be 0.3 mm/sec .

5.2. Discussion

A comparison of the experimental results displayed in Figs. 9 to 11 with the corresponding theoretical curves (Fig. 2 and Fig. 12) shows good agreement. This is certainly no surprise, since the only unknown factors involved in the experiment are the magnetic properties of source and absorber foils. There is no doubt that the assumptions underlying the calculations in Sec. 3 are correct. The main facts which can be learned from the present experiment then are:

- (1) The Mössbauer effect can be used to produce and detect circularly polarized gamma-ray components. The equipment required is quite simple.
- (2) The techniques discussed can, hopefully, be used to investigate the direction of magnetic fields in solids, and their saturation properties.
- (3) The use of polarized sources and absorbers can facilitate the investigation of complicated Mössbauer spectra by reducing the intensity or even extinguishing selected lines.

ACKNOWLEDGMENTS

We would like to thank Dr. Paul Craig and Dr. Paul Barrett for many helpful discussions.